THE JOURNAL OF PHYSICAL CHEMISTRY A

Article

Cite This: J. Phys. Chem. A 2018, 122, 4920−4934

pubs.acs.org/JPCA

A Theoretical Study of Pyrolysis of *exo*-Tetrahydrodicyclopentadiene and Its Primary and Secondary Unimolecular Decomposition Products

Alexander N. Morozov,[†] Alexander M. Mebel,*[,†] and Ralf I. Kaiser*[,‡]

[†]Department of Chemistry and Biochemistry, Florida International University, Miami, Florida 33199, United States

[‡]Department of Chemistry, University of Hawaii at Manoa, Honolulu, Hawaii 96822, United States

Supporting Information

ABSTRACT: Theoretical calculations of the rate constants and product branching ratios in the pyrolysis of *exo*-tetrahydrodicyclopentadiene (JP-10) and its initial decomposition products at combustion-relevant pressures and temperatures were performed and compared to the experimental results from the recently reported molecular beam photoionization mass spectrometry study of the pyrolysis of JP-10 (Zhao et al. *Phys. Chem. Chem. Phys.* **2017**, *19*, 15780−15807). The results allow us to quantitatively assess the decomposition mechanisms of JP-10 by a direct comparison with the nascent product distribution—including radicals and thermally labile closed-shell species—detected in the short-residence-time molecular beam photoionization mass spectrometry experiment. In accord with the experimental data, the major products predicted by the theoretical modeling include methyl radical (CH_3), acetylene (C_2H_2), vinyl radical (C_2H_3), ethyl radical (C_2H_5), ethylene (C_2H_4), allyl radical (C_3H_5), 1,3-butadiene (C_4H_6), cyclopentadienyl radical (C_5H_5), cyclopentadiene (C_5H_6), cyclopentenyl radical (C_5H_7), cyclopentene (C_5H_8), fulvene (C_6H_6), benzene (C_6H_6), toluene (C_7H_8), and 5-methylene-1,3-cyclohexadiene (C_7H_8). We found that ethylene, allyl radical, cyclopentadiene, and cyclopentenyl radical are significant products at all combustion-relevant conditions, whereas the relative yields of the other products depend on temperature. The most significant temperature trends predicted are increasing yields of the C2 and C4 species and decreasing yields of the C1, C6, and C7 groups with increasing temperature. The calculated pressure effect on the rate constant for the decomposition of JP-10 via initial C−H bond cleavages becomes significant at temperatures above 1500 K. The initially produced radicals will react away to form closed-shell molecules, such as ethylene, propene, cyclopentadiene, cyclopentene, fulvene, and benzene, which were observed as the predominant fragments in the long-residence-time experiment. The calculated rate constants and product branching ratios should prove useful to improve the existing kinetic models for the JP-10 pyrolysis.

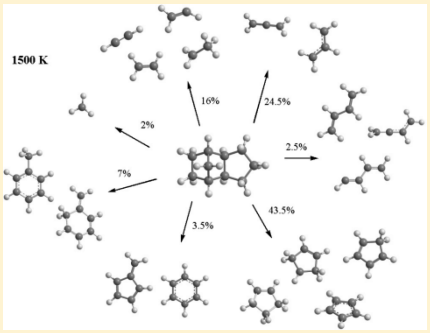

1. INTRODUCTION

The single-component hydrocarbon fuel Jet Propellant-10 (JP-10) is used in detonation engines, missiles, and supersonic combustion ramjets, where a fuel is required to have high thermal stability, high-energy density, and low freezing point. Because of its broad applications, the principal constituent of JP-10, tricyclo[5.2.1.$0^{2,6}$]decane (*exo*-tetrahydrodicyclopentadiene; *exo*-TCD; $C_{10}H_{16}$; Figure 1), has attracted significant attention of researchers, and numerous experimental, theoretical, and modeling studies of its pyrolysis and combustion have been reported in the literature.[1−39] A detailed overview on the JP-10 studies was provided in our recent publication,[40] and here we only briefly reiterate its key points.

The previous studies yielded important information on the formation of closed-shell hydrocarbon intermediates and products in the pyrolysis of JP-10. These species were mainly analyzed off-line and ex situ using gas chromatography−mass spectrometry (GC-MS), which however is not suitable for the detection of radical transient species and thermally labile closed-shell molecules. Consequently, the crucial information on the initial steps of JP-10 pyrolysis—the role and identity of radicals and short living closed-shell intermediates—can be missed. Moreover, the observation of bicyclic polycyclic aromatic hydrocarbons (PAHs) such as naphthalene ($C_{10}H_8$) indicated that consecutive reactions of the initial decomposition products were facilitated by excessive pressures thus changing the "molecular inventory" due to the initial decomposition. In summary, a novel approach probing the open- *and* closed-shell products *online* and in situ is required to overcome the deficiencies of the previous studies.

Recently, we started a combined experimental and theoretical research program focused on the mechanism of the initial decomposition of JP-10.[40] The goal is to provide a detailed input for kinetic modeling of combustion flames in JP-10-based engines. In this project, the pyrolysis experiments were performed in high-temperature reactors to probe the

Received: March 28, 2018
Revised: May 16, 2018
Published: May 17, 2018

DOI: 10.1021/acs.jpca.8b02934
J. Phys. Chem. A 2018, 122, 4920−4934

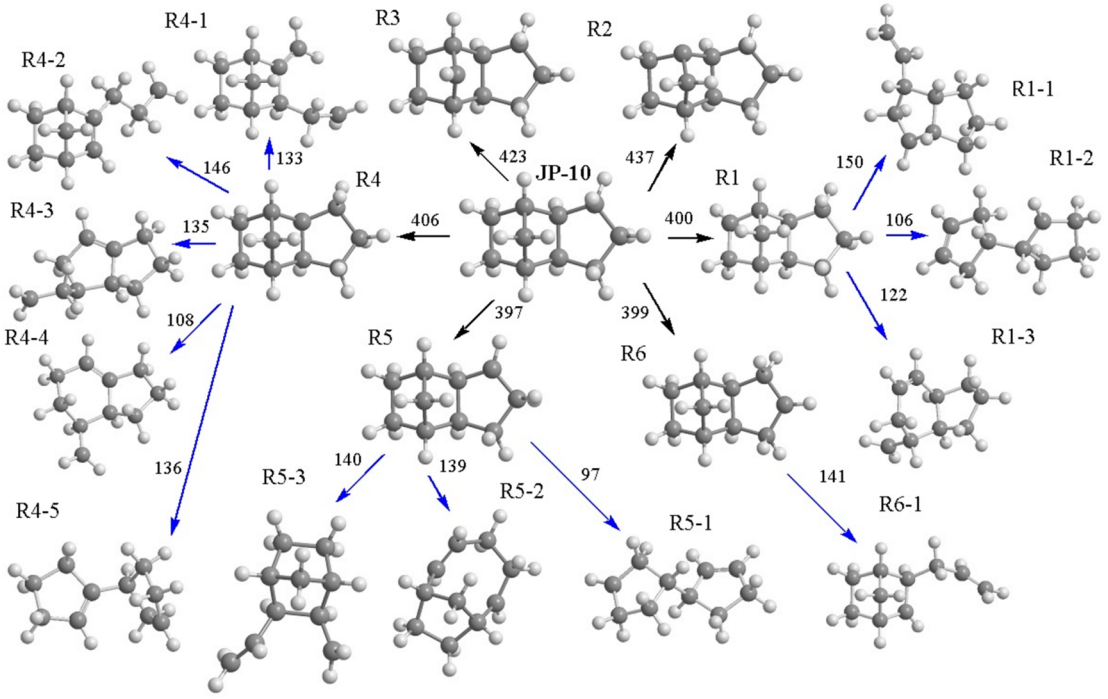

Figure 1. Potential energy diagram for initial decomposition channels of JP-10. The numbers next to black arrows show reaction endothermicities for initial C−H bond cleavages in JP-10. The numbers next to blue arrows show barriers for various initial β-scission processes in the R1 and R4−R6 radicals. All energies calculated at the G3(MP2,CC)//B3LYP/6-311G(d,p) level (given in kJ mol^{-1}).

decomposition of JP-10. Two sets of experiments with residence times of a few 10 μs and of 100 ms were performed under combustion-like temperatures. The emerging product distributions were probed online and in situ in a supersonic molecular beam exploiting soft photoionization with single photon vacuum ultraviolet (VUV) light followed by a mass spectroscopic analysis of the ions in a Re-TOF (TOF = time of flight).[41−58] Our experimental setup allowed detection of thermally labile closed-shell species as well as short living radicals. Molecular beam experiments were combined with high-level electronic structure calculations to study the decomposition of JP-10 over a broad range of combustion-relevant temperatures and pressures systematically. In the present paper we extend our previous theoretical studies of potential energy surfaces (PES) of JP-10 dissociation channels[40] with calculations of rate constants and branching ratios to get a more quantitative insight on the pyrolysis mechanism of JP-10 and to account for the initial molecular inventory required for reliable kinetic modeling of JP-10 oxidation in combustion, which follows the initial pyrolysis step.

The most detailed theoretical calculations on this system prior to our recent work were reported by Vandewiele et al.[17] who employed the automatic Reaction Mechanism Generator (RMG) in conjunction with CBS-QB3 and CASPT2 calculations for the most important decomposition pathways to develop a kinetic model for the JP-10 pyrolysis via various biradical and radical mechanisms. While the kinetic model by Vandewiele et al. was rather successful in the description of the experimental data available at that time, this model appeared to be insufficient to account for the new, more detailed observations utilizing molecular beam photoionization mass spectrometry (MB PIMS) allowing to detect the short living radical and thermally labile closed-shell molecules. The ab initio calculations accompanying the MB PIMS experiments[40] were aimed to find a facile pathway on the pertinent PESs to *every* species (a radical or a molecule) observed experimentally and thus qualitatively explain all the observations. Essentially, the calculations were guided by the MB PIMS experimental data, which provided an unprecedented most detailed molecular inventory in the JP-10 pyrolysis at its initial fast (on a 10−100 μs time scale) stage. The present work moves a step forward and provides temperature- and pressure-dependent rate constants and product branching ratios for all considered reactions and ultimately, relative product yields in the overall pyrolysis process (including the primary and fast secondary and consequent reactions) on the given time scale within the considered mechanisms. The calculated branching ratios are compared with the MB PIMS experimental values, and their trends with temperature are also investigated and reported.

2. COMPUTATIONAL METHODS

For the most part, the PESs for the JP-10 pyrolysis obtained by high-level, chemically accurate ab initio calculations and described previously[40] were used to compute the rate constants and relative product yields presented here. In addition, PESs for several important reaction channels not considered earlier were studied here using the same computational strategy as in the previous work.[40] Briefly, the strategy explores decomposition pathways, where a cleavage of a bond leads directly either to a radical intermediate or to a bimolecular product. This approach is warranted based on a theoretical study by Vandewiele et al., who found that possible biradical pathways are expected to contribute to the total product yield no more than 19%.[7] Optimized Cartesian coordinates and calculated vibrational frequencies of all stationary structures are given in Supporting Information. The energies and molecular properties of local minima and transition states on the PESs pertinent to the

DOI: 10.1021/acs.jpca.8b02934
J. Phys. Chem. A 2018, 122, 4920−4934

unimolecular decomposition of JP-10 and its immediate primary and secondary dissociation products were computed at the G3(MP2,CC)//B3LYP/6-311G(d,p) level of theory.[59−61] T1 diagnostics were checked for each calculated structure during coupled cluster calculations to verify the range of the multireference character of the wave function. It was found that the values never exceeded 0.02 for singlets and 0.03 for doublets thus indicating that the wave functions do not possess a strong multireference character, and hence the CCSD(T) approach should provide adequate energies. To give a reader a sense of typical T1 values, T1 diagnostics on the C_9H_{12} PES (Figure S1 in Supporting Information) are shown for all stationary points. Within the G3(MP2,CC) scheme the computed energetics are expected to provide a chemical accuracy within 10 kJ mol^{-1}. The calculations were performed using the Gaussian 09[62] and MOLPRO 2010[63] program packages.

Rate constants for individual reaction steps were computed using Rice−Ramsperger−Kassel−Marcus (RRKM) theory for unimolecular reactions[64] utilizing the rigid-rotor, harmonic-oscillator (RRHO) model for the calculations of densities of states and partition functions for molecular complexes and the number of states for transition states. For the barrierless reactions such as a C−H bond cleavage in a closed-shell molecule, the flux over a transition state was evaluated within variable reaction coordinate-transition state theory (VRC-TST).[65] In this case the potential energy calculations were performed using the multireference second-order perturbation theory CASPT2 method[66,67] with the cc-pvdz[68] basis set. This method is suitable for a computationally efficient treatment of the multireference character of the wave function for radical−radical reactions.[69] Because of computational limitations, the minimal (2e,2o) active space was a default choice in the CASPT2 calculations, which is generally adequate for the description of static electronic correlation in a process of a single bond cleavage or a reverse process of bond formation from two radicals. A failure in an active space choice could be seen in an irregular character of the calculated minimal energy reaction path (MEP) on a PES for a radical−radical association. For instance, in the case of C_2H_3 + cyclopentenyl (C_5H_7) association—the reverse process for dissociation of 3-vinyl-1-cyclopentene—the calculations with a (2e,2o) active space resulted in a nonmonotonic MEP. In this case, we assumed that all delocalized π orbitals of the C_5H_7 fragment are of importance and need to be included in the active space. In fact, one must include the entire π system, which consists of two π electrons in the C_2H_3 fragment and three π electrons in the C_5H_7 fragment. Together with the unpaired electron in C_2H_3, this resulted in a (6e,6o) active space. The (6e,6o) active space proved to be adequate for the C_2H_3 + C_5H_7 association reaction, as it produced a smooth and monotonic MEP.

Temperature−pressure dependences of the phenomenological rate constants were computed by solving the one-dimensional master equation[70] employing the MESS package.[71] Lennard-Jones parameters (ε, cm^{-1}, σ, Å) = (237, 5.02) needed for the calculation of the pressure dependence of rate constants for the $C_{10}H_x/N_2$ systems were taken from our previous study of the *n*-decane/N_2 system[72] of a similar molecular size. For smaller C_yH_x/N_2 systems (y < 10) we derived the Lennard-Jones parameters using the general rule[73] for calculating these parameters based on the number of carbon atoms using C_{10} parameters as the reference. The "universal" parameters for the hydrocarbons in the nitrogen bath gas, n = 0.86 and α_{300} = 228 cm^{-1},[71] for the temperature dependence of the range parameter α for the deactivating wing of the energy transfer function $\alpha(T) = \alpha_{300}(T/300\ K)^n$ were used in the "exponential down" model[74] of the collisional energy transfer in the master equation. Having the rate constants computed, kinetic equations for a sequence of unimolecular reactions involved in the initial steps of the JP-10 pyrolysis were solved within the steady-state approximation. For the majority of radicals found in the present modeling of the pyrolytic decomposition of JP-10, it was observed that at temperatures above 1000 K the collisional time scales were longer than the time scales for their chemical transformations/decompositions, and chemically significant eigenvalues could not be identified in the master equation, and hence, the corresponding phenomenological pressure-dependent rate constants could not be evaluated. This means that these species are unstable at the high temperatures and rapidly equilibrate ("merge") with their isomerization/decomposition products. In such a case, the pressure-dependent rate constants can be reasonably approximated by the high-pressure (HP) limit rate constants, and consequently, unless a pressure-dependent calculation is specified explicitly, product branching ratios were obtained in the HP limit.

An implementation of the strategy described above and methods to study the complete mechanism of JP-10 pyrolysis is a challenging task due to numerous decomposition pathways with a large number of possible isomers, transition states, and bimolecular products. To overcome this problem we developed a software package, Pyrol, to automate the implementation of our strategy for computational studies of pyrolysis of hydrocarbon molecules. Starting with a closed-shell entity Pyrol first creates a map of all possible initial C−H bond cleavages. If there is a C−C bond cleavage that leads to a direct fragmentation, this channel can be added manually to the reaction map. Next, Pyrol generates input files for Gaussian 09 and MOLPRO 2010 to calculate energies and molecular properties for the species of interest. After the calculations of the initial bond cleavages are finished, the software gathers the results, and a decision whether some of the decomposition channels are too unfavorable and can be excluded can be made. Next, Pyrol analyzes all possible C−C β-scissions in the radicals produced by the initial C−H (C−C) bond cleavages, and the decomposition map is updated accordingly. Again, there is a possibility to edit the map manually to remove or add some desirable channels, such as possibly favorable C−H β-scissions and H migrations. After the decomposition map is updated, the Gaussian 09 and MOLPRO 2010 input scripts for β-scission routes are generated. This process is repeated recursively, until a bond cleavage in each channel ends up with final bimolecular products considered to be stable under given conditions. The resulting PES and calculated molecular properties are then processed by the kinetics facility of Pyrol to generate input files for rate constant calculations by the MESS package. Finally, after the rate constant calculations by MESS are completed, Pyrol solves unimolecular kinetic equations using the steady-state approximation to obtain temperature and pressure dependences for the overall decomposition rate constant and for the product branching ratio.

3. COMPUTATIONAL RESULTS

3.1. Initial C−H Bond Cleavages. The JP-10 molecule decomposition by homolytic cleavage of various C−H bonds can produce six types of $C_{10}H_{15}$ radicals (R1−R6) plus a hydrogen atom.[40] The calculated energetics of these reactions[40]

DOI: 10.1021/acs.jpca.8b02934
J. Phys. Chem. A 2018, 122, 4920−4934

(Figure 1) showed that the R1, R4, R5, and R6 pathways are more favorable, as their computed endothermicities are 397–406 kJ mol^{-1}, as compared to 423 and 437 kJ mol^{-1} for the R3 and R2 pathways, respectively. Consecutively, only decomposition processes to the R1 and R4–R6 radicals were considered here. The calculated rate constants for the C–H bond cleavages at the pressure of 1 atm (Figure 2) exhibit well-

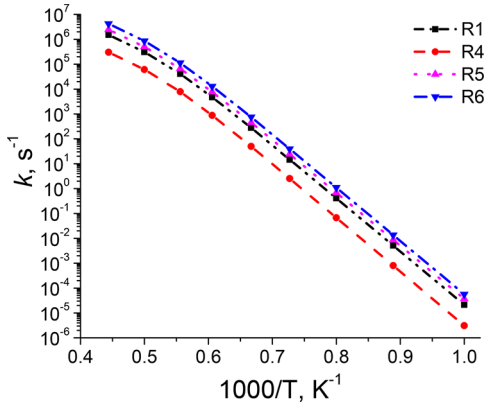

Figure 2. Calculated temperature dependences of rate constants for the main channels of C–H bond clevage in JP-10 ($C_{10}H_{16}$) at 1 atm pressure.

defined Arrhenius behavior and grow from 3.1 × 10^{-6}–5.7 × 10^{-5} s^{-1} at 1000 K to 5 × 10^{1}–7.6 × 10^{2} s^{-1} at 1500 K and to 3 × 10^{5}–4.2 × 10^{6} s^{-1} at 2250 K. These values are in a good agreement with the experimental observation at the Advanced Light Source (ALS) experimental observation[40] that on the 10–100 μs time scale no significant fraction of $C_{10}H_{16}$ is consumed at temperatures below 1000 K, and nearly full decomposition is observed above 1600 K, as the computed lifetime of JP-10 at 1650 K is only ~38 μs. The calculated pressure dependence of the total rate constant for the decomposition of JP-10 via initial C–H bond cleavages is shown in Figure 3. The calculated effect of the pressure increase

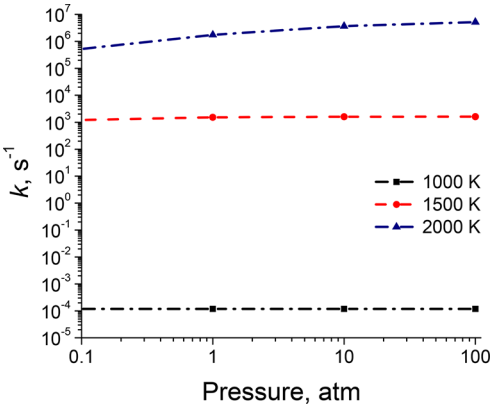

Figure 3. Calculated pressure dependences of the rate constant for the decomposition of JP-10 ($C_{10}H_{16}$) via initial C–H bond cleavages.

from 30 Torr to 100 atm is a 16-fold increase of the rate constant at 2000 K and 1.45-fold increase at 1500 K, whereas no significant pressure effect is observed at 1000 K.

The calculated branching ratios for the R1, R4, R5, and R6 products of the C–H bond cleavages at various temperatures and pressures are summarized in Table 1. Overall, the

Table 1. Calculated Temeprature and Pressure Dependences of the Branching Ratio for the Main Channels of C–H Bond Clevage in JP-10 ($C_{10}H_{16}$)

	T = 1000 K			
	R1	R4	R5	R6
30 Torr	18.1	2.6	31.4	47.9
1 atm	18.1	2.6	31.4	47.9
10 atm	18.1	2.6	31.4	47.9
100 atm	18.1	2.6	31.4	47.9
	T = 1500 K			
	R1	R4	R5	R6
30 Torr	18.1	3.2	29.7	48.9
1 atm	18.1	3.3	29.6	49.1
10 atm	18.1	3.3	29.6	49.1
100 atm	18.1	3.3	29.5	49.1
	T = 2000 K			
	R1	R4	R5	R6
30 Torr	18.0	3.4	29.3	49.3
1 atm	17.9	3.5	29.0	49.6
10 atm	17.8	3.6	28.8	49.8
100 atm	17.7	3.6	28.7	50.0

calculations showed that R1, R5, and R6 are expected to be the predominant channels for the JP-10 pyrolysis. The branching ratio shows little dependence on both temperature and pressure. Importantly, the branching ratio calculations support our computational strategy, as contributions of the R2 and R3 channels are expected to be an order of magnitude lower than that of the R4 channel and thus of no significance for accounting for the molecular inventory of the JP-10 pyrolytic process. Following the initial C–H bond cleavages, all possible C–C bond β-scissions in R1 and R4–R6 radicals were outlined in our previous work[40] and are shown here in Figure 1. The intermediates accessed after first β-scissions can further isomerize or dissociate giving a variety of JP-10 pyrolytic products. PES calculations for the R1 and R4–R6 dissociation channels were performed and explained in great detail in our previous work (Figures 16–22 and computational results in ref 40), which allows us to proceed here with kinetic calculations of rate constants and product branching ratios.

3.2. Decomposition of the R1 Radical. By initial C–C β-scission R1 can isomerize to the radical intermediates R1–1, R1–2, and R1–3 via barriers of 150, 106, and 122 kJ mol^{-1}, respectively (Figure 1).[40] Ultimately, after various isomerization processes,[40] these three radical intermediates decompose into eight primary products shown here in Scheme 1 (primary decompositions are indicated by black arrows), which include methyl, CH_3, vinyl, C_2H_3, cyclopentenyl, C_5H_7, 1,4-pentadien-5-yl, C_5H_7, C_6H_9, cyclopentene-allyl, C_8H_{11} radicals and ethylene, C_2H_4, 1,3-butadiene, C_4H_6, cyclopentene,C_5H_8, as well as C_8H_{12} and C_9H_{12} closed-shell fragments. The calculated rate constant for the primary decomposition of the R1 radical is shown in Figure 4. The rate constant grows from 7.2 × 10^{6} s^{-1} at 1000 K to 3.6 × 10^{11} s^{-1} at 2500 K. Thus, in this temperature range, R1 is expected to undergo full decomposition on the time scale of the ALS experiment (10–100 μs). Table 2 shows the branching ratios for the eight products of the primary decomposition of the R1 radical described above calculated in the 1000–2500 K temperature range. The calculations showed that at 1000 K R1 yields mainly cyclopentenyl radical, C_5H_7 + cyclopentene, C_5H_8 (R1–2_p1). With increasing temperature,

DOI: 10.1021/acs.jpca.8b02934
J. Phys. Chem. A 2018, 122, 4920–4934

Scheme 1. Primary and Secondary Channels of Decomposition of R1

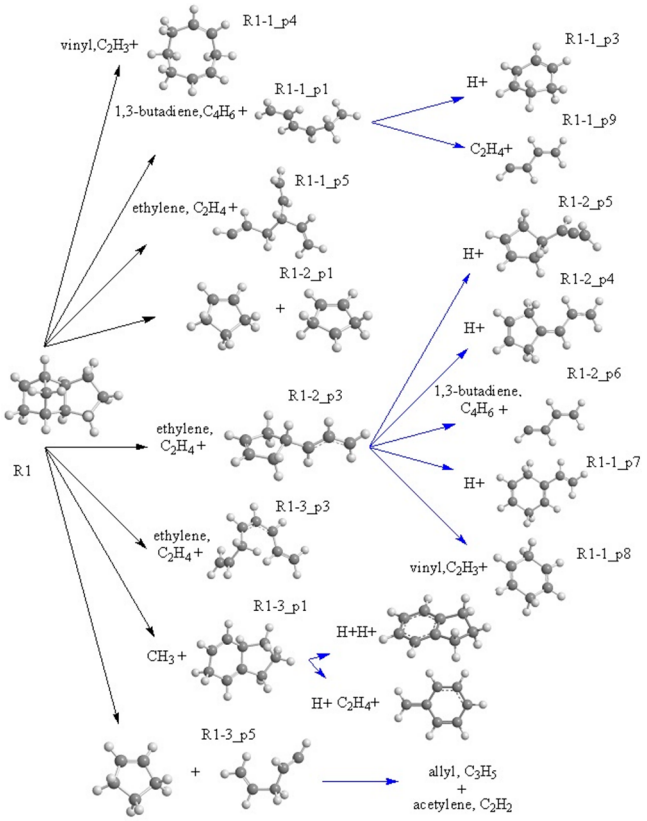

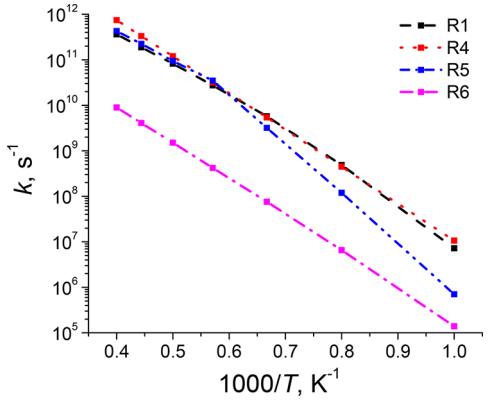

Figure 4. Calculated rate constants for the primary decompositions of the R1 and R4−R6 radicals.

the relative yield of R1−2_p1 falls, whereas the yields of ethylene, C_2H_4 + cyclopentene-allyl, C_8H_{11} (R1−2_p3) and cyclopentene, C_5H_8 + 1,4-pentadien-5-yl, C_5H_7 (R1−3_p5) increase. The yield of R1−1_p1, another significant product, which consists of 1,3-butadiene, C_4H_6 + C_6H_9 (R1−1_p1), fluctuates in the 5.3−12.8% range without a definitive temperature trend. The yield of the methyl radical, CH_3 + C_9H_{12} (R1−3_p1) product steadily grows with temperature to reach 1.1% at 2500 K, which translates into ∼0.2% maximal contribution to the total molecular inventory of the JP-10 pyrolysis. In the present study, the PES for the R1 decomposition reported in the previous work was extended to include the decomposition of the C_9H_{12} (R1−3_p1) closed-shell fragment. The result is shown in Figure S1 in Supporting Information. The calculations showed that C_9H_{12} (R1−3_p1) will decompose further to H + H + indane, C_9H_{10} (which would eventually decay to indene, C_9H_8), and ethylene, C_2H_4 + benzyl radical, C_7H_7 + H. This is in an accord with our experiment, where indane, indene, and toluene (a product of benzyl + H recombination) were observed as trace products. On the basis of the calculated branching ratios, R1−1_p4, R1−1_p5, and R1−3_p3 were deemed as insignificant products in the total molecular inventory of the JP-10 pyrolysis, with each of them contributing ∼0.1%. It is worth noting that the low-yield fragment C_8H_{12} (R1−1_p4) is a precursor for the experimentally observed trace product 1,3,5-cyclooctatriene, C_8H_{10}.

Under typical combustion temperatures, the radical fragments 1,4-pentadien-5-yl, C_5H_7, C_6H_9, and cyclopentene-allyl, C_8H_{11} are expected to undergo rapid secondary decompositions. This is confirmed by the ALS experiment,[40] where the aforementioned radicals were not observed. Products of the secondary decompositions (indicated by blue arrows in Scheme 1) must be accounted for a proper modeling of JP-10 combustion flames. Let us start with the secondary fragmentation of the 1,4-pentadien-5-yl radical, C_5H_7 (R1−3_p5), which leads to the acetylene, C_2H_2 + allyl, C_3H_5 product.[40] The calculated rate constant for this proces is shown in Figure 5. The rate constant increases from 7.9×10^6 s^{-1} at 1000 K to 1.9×10^{12} s^{-1} at 2500 K. Thus, 1,4-pentadien-5-yl is expected to undergo full decomposition on the time scale of the ALS experiment. Indeed, significant yields of both allyl and acetylene were detected in the experiment.[40]

The C_6H_9 radical (R1−1_p1) dissociates further either by β-scission to ethylene, C_2H_4 + C_4H_5 via a 157 kJ mol^{-1} barrier for the C_2H_4 loss or via a 45 kJ mol^{-1} barrier for the reverse β-scission, that is, a six-member ring closure, to H + 1,3-cyclohexadiene, C_6H_8.[40] The calculated branching ratio (Table 3) for these products shows a strong temperature trend. The

Table 2. Calculated Branching Ratio for the Primary Decomposition of R1

	temperature						
product	1000 K	1250 K	1500 K	1750 K	2000 K	2250 K	2500 K
C_2H_3 + C_8H_{12} (R1−1_p4)	0	0	0	0.1	0.2	0.5	0.7
C_4H_6 + C_6H_9 (R1−1_p1)	5.3	12.1	11	10.5	11	11.9	12.8
C_2H_4 + C_8H_{11} (R1−1_p5)	0	0	0	0.1	0.2	0.3	0.4
C_5H_7 + C_5H_8 (R1−2_p1)	89.4	76.3	68.9	63	57.7	53.2	49.3
C_2H_4 + C_8H_{11} (R1−2_p3)	4.7	8.7	12.8	16.5	19.5	21.9	23.7
C_2H_4 + C_8H_{11} (R1−3_p3)	0	0.2	0.4	0.5	0.6	0.6	0.6
CH_3 + C_9H_{12} (R1−3_p1)	0.3	0.4	0.5	0.6	0.8	0.9	1.1
C_5H_7 + C_5H_8 (R1−3_p5)	0.2	2.3	6.3	8.7	10	10.8	11.4

DOI: 10.1021/acs.jpca.8b02934
J. Phys. Chem. A 2018, 122, 4920−4934

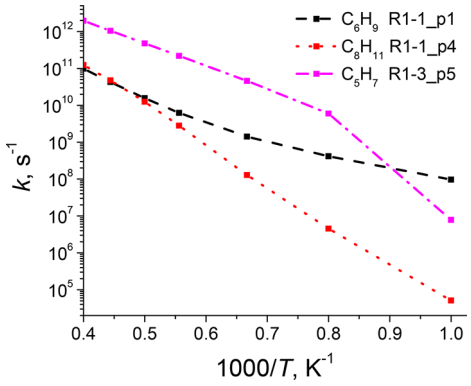

Figure 5. Calculated rate constants for the secondary decompositions in the R1 channel.

lower-barrier pathway to H + 1,3-cyclohexadiene, C_6H_8, dominates at 1000 K, while with growing temperature this product is replaced by $C_2H_4 + C_4H_5$ due to a higher entropy of the latter pathway. The C_4H_5 radical formed here can serve as a precursor for both 1,2,3-butatriene and vinylacetylene. The rate constant for the secondary decomposition of the C_6H_9 radical is shown in Figure 5. The rate constant increases from 9.7×10^7 s^{-1} at 1000 K to 9.9×10^{10} s^{-1} at 2500 K, which confirms that the decomposition of C_6H_9 (R1−1_p1) is faster than the time scale of 10 μs. This is in line with the experimental results, where the C_6H_9 radical was not detected; instead, its fragmentation products such as 1,3-cyclohexadiene, butatriene, and vinylacetylene were observed.[40]

PES for the secondary decomposition of the cyclopentene-allyl, C_8H_{11} radical fragment of the R1−2_p3 product was described in great detail in the previous work.[40] In summary, H-loss pathways to the H + C_8H_{10} (R1−2_p5, R1−2_p4) products via barriers of 172 and 243 kJ mol^{-1}, respectively, compete with a five-member ring opening via a barrier of 131 kJ mol^{-1} and subsequent fragmentation via a barrier of 266 kJ mol^{-1}, which leads to the 1,3-butadiene, $C_4H_6 + C_4H_5$ (R1−2_p6) product. Alternatively, the five-member ring opening can be followed by a six-member ring closure via a barrier of 166 kJ mol^{-1} to the intermediate, which is a precursor of the H + 2,5-dihydrostyrene, C_8H_{10} (R1−1_p7) and vinyl, C_2H_3 + 1,4-cyclohexadiene, C_6H_8 (R1−1_p8) products. The calculated temperature dependence of the branching ratio for the products described above is presented in Table 4. The result shows that the relative yields of the products strongly depend on temperature. The R1−2_p4 product of the direct H loss, H + C_8H_{10}, prevails at 1000 K followed by vinyl, C_2H_3, + 1,4-cyclohexadiene, C_6H_8 (R1−1_p8) and H + 2,5-dihydrostyrene, C_8H_{10} (R1−1_p7). At higher temperatures, the yield of these products becomes low as compared to the yield of the higher-entropy 1,3-butadiene, C_4H_6, + C_4H_5 (R1−2_p6) product. The calculated low yields of 2,5-dihydrostyrene, C_8H_{10}, and 1,4-cyclohexadiene, C_6H_8, are in accord with the fact that in experiment styrene (2,5-dihydrostyrene is a precursor of styrene) and 1,4-cyclohexadiene were observed in trace quantities.[40]

In summary, R1 is the third largest contributor (~18% of the total molecular inventory) to the products of the JP-10 pyrolysis. The calculations predict that at temperatures of interest, R1 largely yields the five-member ring products cyclopentene and cyclopentenyl. R1 also provides small yields of cyclohexadienes, toluene, styrene, cyclooctatriene, and indane. The yield of smaller fragments such as methyl, vinyl, allyl, acetylene, ethylene, and 1,3-butadiene, produced in a variety of the R1 decomposition channels, shows a tendency to grow with increasing temperature.

3.3. The R4 Radical. Initial isomerization of the R4 radical can proceed by five C−C β-scission channels via barriers ranging from 108 to 146 kJ mol^{-1} and leading to the five intermediates R4−1−R4−5 (Figure 1). Secondary isomerization of these intermediates, including H migrations, was studied in our previous work,[40] where six primary products of the initial decomposition of the R4 radical were identified (Scheme 2). The primary decomposition of R4 is the source of the experimentally observed methyl, CH_3 (R4−4_p1), ethyl, C_2H_5 (R4−3_p1), and allyl, C_3H_5 (R4−5_p1), radicals. The larger C_5H_7 (R4−5_p2) and C_8H_{11} (R4−1_p1, R4−3_p2) radical fragments were not detected, and hence, their secondary decomposition on the ALS experimental time scale is implicated to be fast. The inventory of the closed-shell fragments produced in the primary decomposition of R4 consists of ethylene, C_2H_4 (R4−1_p1, R4−3_p2), C_5H_8 (R4−5_p2), C_7H_{10} (R4−5_p1), C_8H_{10} (R4−3_p1), and C_9H_{12} (R4−4_p1). Figure 4 shows the calculated temperature dependence of the rate constant for the primary decomposition of the R4 radical. The rate constant grows from 1.6×10^7 s^{-1} at 1000 K to 7.4×10^{11} s^{-1} at 2500 K. Similar to R1, the primary C−C β-scissions in R4 is a fast process relative to the experimental time scale of 10−100 μs. The temperature dependence of the calculated branching ratio for the products of the primary decomposition of R4 is shown in Table 5. The ethylene, C_2H_4, and two different C_8H_{11} (R4−1_p1, R4−3_p2) radicals account for ~70% of the overall yield in the 1000−2500 K temperature range. The yield of the R4 → R4−3_p1 channel (ethyl, C_2H_5, + C_8H_{10}) decreases with increasing temperature from 23.8% at 1000 K to 2.8% at 2500 K. This channel involves entropically unfavorable H-migration steps, which are less competitive at higher temperatures as compared to the channels leading to C_2H_4 elimination. The yields of the methyl, CH_3 + C_9H_{12} (R4−4_p1) and of allyl, C_3H_5 + C_7H_{10} (R4−5_p1) products steadily grow with temperature from 1.5 to 18.2% and from 5 to 12.3%, respectively. Since at temperatures and pressures of interest R4 itself is a low-yield channel (less than 4%), the low-yield R4−5_p2 product (less than 0.1% of all products of the R4 decomposition) was deemed as not significant for the total molecular inventory of the JP-10 pyrolysis.

Let us first briefly describe the secondary decomposition of the C_8H_{11} (R4−1_p1) radical fragment (Figure 19 in ref 40).

Table 3. Calculated Branching Ratio for the Secondary Decomposition of R1-1_p1

	temperature						
product	1000 K	1250 K	1500 K	1800 K	2000 K	2250 K	2500 K
H + 1,3-cyclohexadiene, C_6H_8	99.3	91.9	66.9	32.1	18.6	9.9	5.7
C_4H_5 + ethylene, C_2H_4,	0.7	8.1	33.1	67.9	81.4	90.1	94.3

DOI: 10.1021/acs.jpca.8b02934
J. Phys. Chem. A 2018, 122, 4920−4934

Table 4. Calculated Branching Ratio for the Secondary Decomposition of Cyclopentene-Allyl, C_8H_{11} (R1-2_p3)

	temperature						
product	1000 K	1250 K	1500 K	1750 K	2000 K	2250 K	2500 K
H + C_8H_{10} (R1−2_p5)	0	0.3	0.6	0.8	1.1	1.6	2.4
H + C_8H_{10} (R1−2_p4)	62.5	58.2	39.7	21.8	17.2	15.8	16.6
C_4H_6 + C_4H_5 (R1−2_p6)	1.5	14.3	44.7	71.7	78.7	81.1	80.2
H + C_8H_{10} (R1−1_p7)	10.9	6.6	3.2	1	0.5	0.2	0.1
C_2H_3 + C_6H_8 (R1−1_p8)	25.1	20.6	11.8	4.7	2.5	1.3	0.7

Scheme 2. Primary and Secondary Channels of Decomposition of R4

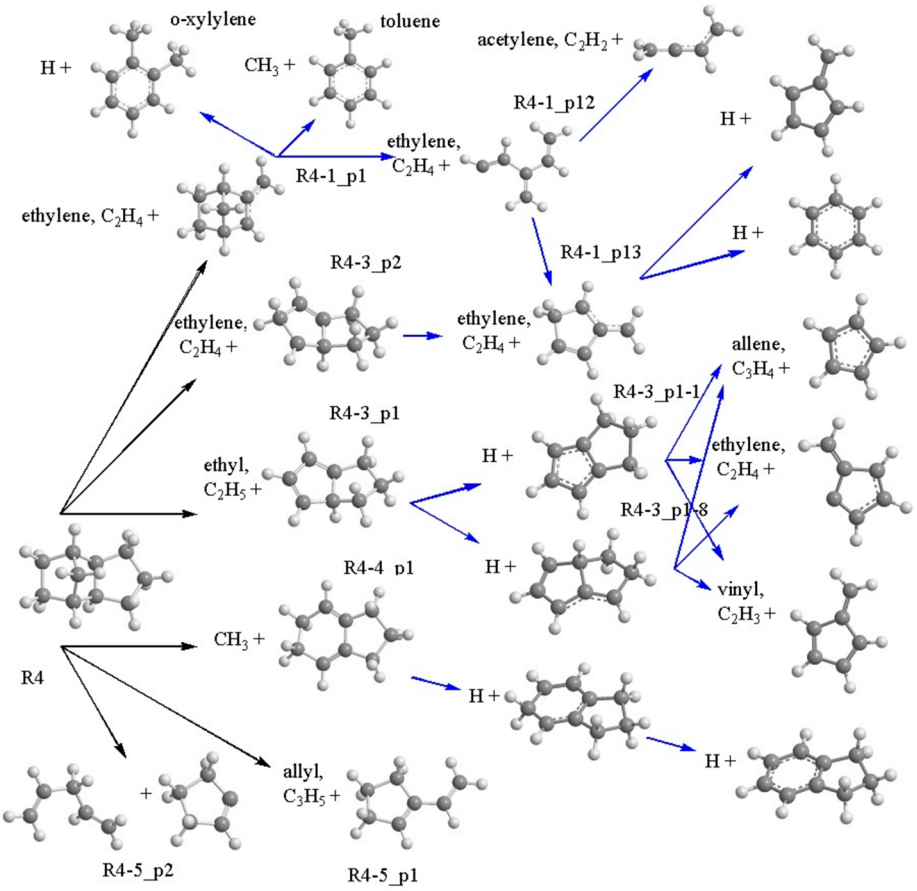

Table 5. Calculated Branching Ratios for the Primary Decomposition of R4

	temperature						
product	1000 K	1250 K	1500 K	1750 K	2000 K	2250 K	2500 K
C_2H_4 + C_8H_{11} (R4−1_p1)	58.4	53.5	49.2	46.3	44.3	43.2	42.6
C_2H_4 + C_8H_{11} (R4−3_p2)	11.4	18.5	22	23.4	23.7	23.8	23.9
C_2H_5 + C_8H_{10} (R4−3_p1)	23.8	14.3	9	6.1	4.4	3.5	2.8
CH_3 + C_9H_{12} (R4−4_p1)	1.5	4	7.6	11.5	14.8	17	18.2
C_3H_5 + C_7H_{10} (R4−5_p1)	5	9.8	12.2	12.8	12.7	12.5	12.3
C_5H_7 + C_5H_8 (R4−5_p2)	0	0	0	0	0	0.1	0.1

The β-scission process, which breaks the bicyclic framework and produces a six-member ring with two out-of-ring CH_2 groups, is followed either by a series of energetically favorable 1,2-H migrations or by a series of entropically favorable C−C bond β-scissions. The H-migration pathway eventually leads either to the H + *o*-xylene, C_8H_{10} or methyl, CH_3 + toluene, C_7H_8 products. The C−C bond β-scission pathway leads first to ethylene, C_2H_4 + C_6H_7 (R4−1_p12), which can either dissociate to acetylene, C_2H_2 + C_4H_5 or form a five-member ring product R4−1_p13. R4−1_p13 is a known precursor for H + fulvene, C_6H_6 and H + benzene, C_6H_6.[75] The barrier for the five-member ring closure pathway is 111 kJ mol^{-1} lower than the barrier to the higher entropy C_2H_2 + C_4H_5 product. An interplay of enthalpy versus entropy in the channels described above results in a strong temperature dependence of the calculated branching ratios (Table 6). At 1000 K, the pyrolysis of the C_8H_{11} radical (R4−1_p1) yields mainly (97.5%) atomic hydrogen and *o*-xylene; at 1500 K, the

DOI: 10.1021/acs.jpca.8b02934
J. Phys. Chem. A 2018, 122, 4920−4934

Table 6. Calculated Branching Ratios for the Secondary Decomposition of R4-1_p1 (C_8H_{11})

	temperature						
product	1000 K	1250 K	1500 K	1750 K	2000 K	2250 K	2500 K
H + *o*-xylene, C_8H_{10}	97.50	74.70	35.10	15.50	9.20	7.30	6.70
CH_3 + toluene, C_7H_8	0.00	0.00	0.00	0.00	0.00	0.00	0.00
C_2H_4 + C_2H_2 + C_4H_5	0.01	0.83	13.69	45.55	70.91	82.87	88.08
C_2H_4 + H + fulvene, C_6H_6	0.04	1.75	10.64	15.72	11.71	7.14	4.20
C_2H_4 + H + benzene, C_6H_6	2.46	22.72	40.56	23.24	8.17	2.69	0.93

ethylene, C_2H_4 + H + C_6H_6 (fulvene or benzene) products account for ~50% of the products; and at temperatures above 2000 K, the highly fragmented ethylene, C_2H_4 + acetylene, C_2H_2 + C_4H_5 product becomes prevalent (88% at 2500 K). The C_4H_5 radical fragment was not observed directly in the ALS experiment, but it serves as a precursor of vinylacetylene and 1,2,3-butatriene observed at high temperatures.[40] The computed rate constants for the secondary decompositions of the C_8H_{11} (R4−1_p1) and the C_6H_7 (R4−1_p12) radicals are presented in Figure 6. The calculations show that the secondary

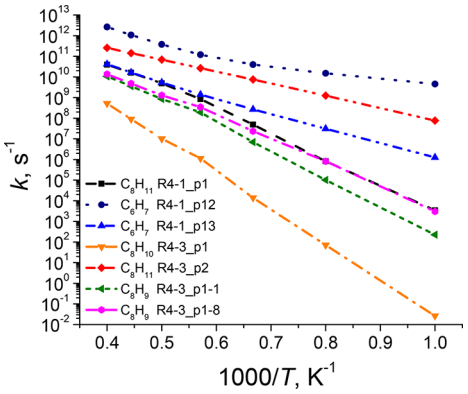

Figure 6. Calculated rate constants for the secondary decompositions in the R4 channel.

decomposition of C_8H_{11} (R4−1_p1) is relatively slow at lower temperatures of interest (3.5×10^3 s^{-1} at 1000 K). On the 10 μs time scale full decomposition of the C_8H_{11} (R4−1_p1) radical is achievable at 1250 K and higher temperatures (8.2×10^5 s^{-1} at 1200 K; 3.9×10^{10} s^{-1} at 2500 K). Regarding the C_6H_7 (R4−1_p12) radical, the 1000 K temperature is high enough for its full decomposition on the experimental time scale (4.5×10^9 s^{-1} at 1000 K and 2.6×10^{12} s^{-1} at 2500 K).

The secondary decomposition of the C_8H_{11} radical (R4−3_p2) proceeds by two consecutive β-scissions. The first one results in five-member ring opening, and the second leads to ethylene, C_2H_4 + C_6H_7 (R4−1_p13) and finally to the experimentally observed fulvene and benzene.[40] The calculated rate constants for the secondary decompositions of the C_8H_{11} (R4−3_p2) and C_6H_7 (R4−1_p13) radicals are shown in Figure 6. The calculations predict that the secondary decomposition of the C_8H_{11} (R4−3_p2) fragment is very fast, with the rate constant changing from 7.7×10^7 s^{-1} at 1000 K to 2.6×10^{11} s^{-1} at 2500 K. The rate constant for the secondary decomposition of the C_6H_7 (R4−1_p13) radical increases from 1.2×10^6 s^{-1} at 1000 K to 4.8×10^{10} s^{-1} at 2500 K. The calculated branching ratio for the secondary decomposition of the C_8H_{11} (R4−3_p2) radical to the products containing fulvene and benzene (Table 7) shows that benzene eventually concedes to fulvene as the temperature grows from 1000 to 2500 K.

PES for the decomposition of the C_8H_{10} (R4−3_p1) closed-shell fragment was not calculated previously and is presented here in Figure S2 (Supporting Information). This secondary decomposition proceeds by H-loss, C_8H_{10} (R4−3_p1) → H + C_8H_9 (R4−3_p1−1, R4−3_p1−8). The rate constant for this process was calculated to be relatively slow (Figure 6). After the H-loss, the C_8H_9 radicals (R4−3_p1−1 and R4−3_p1−8) undergo five-member ring opening followed either by a fragmentation to ethylene, C_2H_4 + fulvenyl radical, C_6H_5 or to vinyl, C_2H_3 + fulvene, C_6H_6. There is also an alternative pathway to the allene, C_3H_4 + cyclopentadienyl, C_5H_5 product. However, in addition to the C−C β-scission, before the fragmentation this pathway requires two H-migrations. The calculated branching ratios (Table 8) for the secondary decomposition of R4−3_p1 predict that only the C_2H_x and C_6H_x fragments are formed in the 1000−2500 K temperature range. The calculations showed that the yield of ethylene, C_2H_4 + fulvenyl radical, C_6H_5 grows with increasing temperature.

In this work we also performed PES calculations for the secondary decomposition of the C_9H_{12} (R4−4_p1) closed-shell fragment. The resulting surface is shown in Figure S3 (Supporting Information). The calculations predict that the pyrolysis of C_9H_{12} (R4−4_p1) mainly proceeds by two consecutive H-losses to yield H + H + indane, C_9H_{10}. Finally, since R4 itself yields less than 4% of the molecular inventory of the JP-10 pyrolysis (Table 1), we do not consider here secondary fragmentations in the low-yield channels, such as further decompositions of R4−5_p1 and R4−5_p2.

To summarize, the R4 channel is the least important of the channels of the JP-10 pyrolysis considered here. The yield of this channel varies in the 2.6−3.6% range at the temperatures and pressures of interest. The R4 channel is a source of the experimentally observed methyl, ethyl, and allyl radicals. The computed molecular inventory of the R4 decomposition includes some major closed-shell molecules (ethylene, fulvene, and benzene) observed in the experiment. R4 also yields the

Table 7. Calculated Branching Ratios for the Secondary Decomposition of the C_8H_{11} (R4-3_p2) Radical

	temperature						
product	1000 K	1250 K	1500 K	1750 K	2000 K	2250 K	2500 K
C_2H_4 + H + fulvene, C_6H_6	1.4	7.2	20.8	40.3	58.8	72.6	81.7
C_2H_4 + H + benzene, C_6H_6	98.6	92.8	79.2	59.7	41.2	27.4	18.3

DOI: 10.1021/acs.jpca.8b02934
J. Phys. Chem. A 2018, 122, 4920−4934

Table 8. Calculated Branching Ratios for the Secondary Decomposition of C_8H_{10} (R4-3_p1)

	temperature						
product	1000 K	1250 K	1500 K	1750 K	2000 K	2250 K	2500 K
H + C_2H_4 + fulvenyl, C_6H_5	13.2	43.1	64.4	70.3	70.7	70.2	69.6
H + C_2H_3 + fulvene, C_6H_6	86.8	56.9	35.6	29.7	29.3	29.8	30.4
H + C_2H_4 + cyclopentadienyl, C_5H_5	0.0	0.0	0.0	0.0	0.0	0.0	0.0

Scheme 3. Primary and Secondary Channels of Decomposition of R5-1

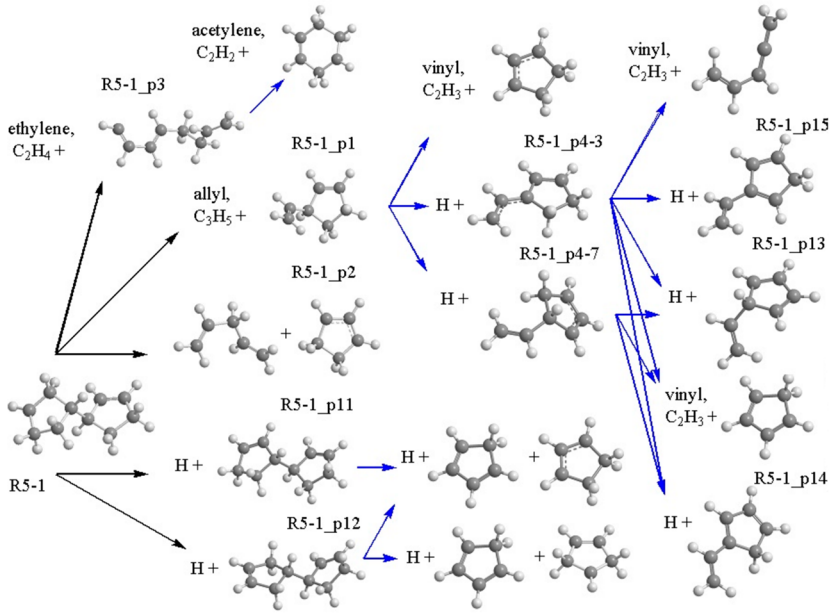

Table 9. Calculated Branching Ratios for the Primary Decomposition of R5

	temperature						
product	1000 K	1250 K	1500 K	1750 K	2000 K	2250 K	2500 K
C_3H_5 + C_7H_{10} (R5−1_p1)	32.4	29.5	26.9	24.1	22.3	20.0	18.0
C_2H_4 + C_8H_{11} (R5−1_p3)	0.0	0.0	0.1	0.6	1.2	2.2	3.1
C_5H_7 + C_5H_8 (R5−1_p2)	4.4	5.0	5.3	5.4	5.4	5.4	5.4
H + $C_{10}H_{14}$ (R5−1_p11)	24.4	26.0	27.2	28.4	29.0	29.6	30.1
H + $C_{10}H_{14}$ (R5−1_p12)	38.7	39.7	40.5	41.7	42.1	42.7	43.3

minor products *o*-xylene and toluene (R4−1_p1), indane and indene (R4−4_p1), as well as fulveneallene and fulveneallenyl (R4−5_p1). The relative product yields in the R4 channel are predicted to depend significantly on temperature; that is, the reaction flux to the products containing six-member ring fragments in the lower temperature range shifts to the products containing five-member fragments when the temperature increases to the combustion relevant range.

3.4. The R5 Radical. The R5 radical can undergo three possible C−C bond β-scissions via barriers of 97−140 kJ mol^{-1} forming R5−1, R5−2, and R5−3 (Figure 1). The decomposition of R5 via R5−1 is favored over the channels via R5−2 or R5−3. Consequently, only pathways involving R5−1 were studied in our previous work (see Figure 21 in ref 40) and are shown here in Scheme 3. The inventory of radicals produced in the primary decomposition of R5−1 includes allyl, C_3H_5 (R5−1_p1), cyclopentenyl, C_5H_7 and the open-chain C_8H_{11} (R5−1_p3) fragment. The inventory of closed-shell fragments in the primary decomposition of R5−1 consists of ethylene, C_2H_4 (R5−1_p3), 3-vinyl-1-cyclopentene, C_7H_{10} (R5−1_p1), 1,4-pentadiene, C_5H_8 (R5−1_p2), and of two $C_{10}H_{14}$ (R5−1_p11, R5−1_p12) fragments.

Let us briefly describe five primary channels of R5−1 decomposition. There are two C−C bond β-scission pathways where a five-member ring is breached first. This can be followed by a fragmentation to allyl, C_3H_5 + 3-vinyl-1-cyclopentene, C_7H_{10} (R5−1_p1). Alternatively, after the first β-scission, R5−1 can also dissociate to cyclopentenyl, C_5H_7 + 1,4-pentadiene, C_5H_8 (R5−1_p2). 1,4-Pentadiene was not observed in the ALS experiment, likely because it can be easily interconverted into significantly more stable C_5H_8 isomers cyclopentene (a significant product observed in experiment) and 1,3-pentadiene (a trace product). There is also a high barrier pathway where the first β-scission is followed by another one leading to the open-chain $C_{10}H_{15}$ intermediate and finally to ethylene, C_2H_4 + C_8H_{11} (R5−1_p3). It turned out that in addition to the previously studied C−C β-scission pathways of R5−1 decomposition, H-loss also provides two viable channels leading to the H + $C_{10}H_{14}$ (R5−1_p11, R5−1_p12) products (the updated PES for the decomposition of R5−1 is given in Figure S4 in Supporting Information). The calculated temper-

DOI: 10.1021/acs.jpca.8b02934
J. Phys. Chem. A 2018, 122, 4920−4934

Table 10. Calculated Branching Ratio for the Secondary Decomposition of C_7H_{10} (R5-1_p1)

product	temperature						
	1000 K	1250 K	1500 K	1750 K	2000 K	2250 K	2500 K
C_2H_3 + cyclopentenyl, C_5H_7	0.0	0.0	0.6	4.4	10.4	21.5	33.9
H + C_2H_3 + penta-1,2,4-triene, C_5H_6	0.0	0.0	0.3	2.0	4.1	6.0	6.1
H + C_2H_3 + cyclopentadiene, C_5H_6	2.9	7.8	14.8	23.0	26.4	27.8	26.6
H + H + C_7H_8 (R5−1_p13)	0.3	0.6	1.0	1.7	2.1	2.3	2.4
H + H + C_7H_8 (R5−1_p14)	55.5	48.4	41.8	33.5	27.4	20.4	15.0
H + H + C_7H_8 (R5−1_p15)	41.3	43.2	41.4	35.3	29.4	21.9	16.0

ature dependence of the rate constant for the primary decomposition of the R5 radical is shown in Figure 4. The results (7.3×10^5 s^{-1} at 1000 K to 4.3×10^{11} s^{-1} at 2500 K) show that the decomposition of the radical R5 is somewhat slower than those of R1 and R4. However, the temperature of 1200 K and higher is sufficient for full primary decomposition of R5 on the time scale of the ALS experiment. The temperature dependence of the calculated branching ratios for the primary products of the R5 decomposition is shown in Table 9. The calculations predict that in the 1000−2500 K temperature range, allyl, C_3H_5 + 3-vinyl-1-cyclopentene, C_7H_{10} (R5−1_p1), and H + $C_{10}H_{14}$ (R5−1_p11, R5−1_p12) are the main products of the primary decomposition of R5. Since the C_7H_{10}, C_8H_{11}, and $C_{10}H_{14}$ fragments were not observed in the ALS experiment, we proceed below with consideration of their secondary decompositions.

Let us start first with the C_8H_{11} radical, which is produced in the low-yield R5−1_p3 channel (Table 9). C_8H_{11} undergoes a high-barrier C−C bond β-scission leading to acetylene, C_2H_2 and the open-chain C_6H_9 product. After that, through a reverse β-scission, a six-member ring radical, C_6H_9, is formed. This radical fragment serves as a precursor for the experimentally observed 1,3- and 1,4-cyclohexadiene isomers.[40]

Second, both of the $C_{10}H_{14}$ closed-shell fragments (R5−1_p11, R5−1_p12) have the same mechanism of the secondary decomposition. It starts with an H-loss, which is followed by β-scission of the C−C bond connecting two five-member rings. The final products of the $C_{10}H_{14}$ (R5−1_p11, R5−1_p12) secondary decomposition include H, cyclopentadiene, C_5H_6, and two isomers of the cyclopentenyl, C_5H_7 radical.

Lastly, the secondary decomposition of 3-vinyl-1-cyclopentene, C_7H_{10} (R5−1_p1) produces H, vinyl, C_2H_3, 1,2,4-pentatriene, C_5H_6, cyclopentadiene, C_5H_6, cyclopentenyl, C_5H_7, and several C_7H_8 closed-shell fragments. The calculated PES for the secondary decomposition of C_7H_{10} (R5−1_p1) is presented in Figure S5 (Supporting Information). The H-loss mechanism here competes with the loss of the vinyl side-chain C_2H_3, which leads to the C_2H_3 + cyclopentenyl, C_5H_7 product. The computed endothermicities for the R5−1_p4−3, R5−1_p4−7 H-loss pathways are 291 and 343 kJ mol^{-1}, respectively, while the computed endothermicities for the loss of the vinyl side chain is 345 kJ mol^{-1}. The C_7H_9 radical fragments (R5−1_p4−3, R5−1_p4−7) can undergo further decomposition, again, either by H-loss leading to the H + C_7H_8 (R5−1_p13, R5−1_p14, and R5−1_p15) products or by the vinyl group elimination leading to the C_2H_3 + cyclopentadiene, C_5H_6 and C_2H_3 + 1,2,4-pentatriene, C_5H_6 products. The calculated temperature dependence of the branching ratios for the secondary decomposition of C_7H_{10} (R5−1_p1) is shown in Table 10. The result reveals that the H + H + C_7H_8 products prevail at lower temperatures. At temperatures above 2000 K, the C_2H_3 + C_5H_7/C_2H_3 + C_5H_6 + H channels become favorable. The calcualted rate constants for the secondary decompositions of the C_7H_{10} (R5−1_p1) and C_7H_9 (R5−1_p4−3, R5−1_p4−7) fragments are presented in Figure 7. As

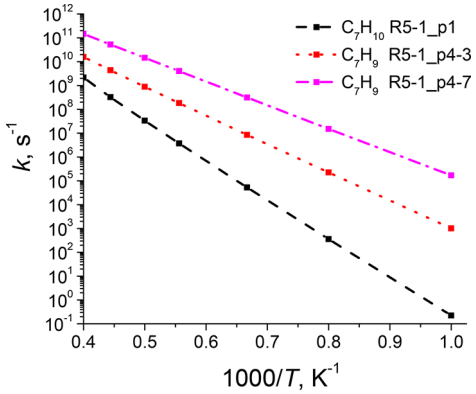

Figure 7. Calculated rate constants for the secondary decompositions in the R5 channel.

one would expect, the secondary decomposition of the closed-shell fragment C_7H_{10} is the rate-limiting process for the R5−1_p1 channel. Temperatures higher than 1500 K are required for the full secondary decomposition of C_7H_{10} (R5−1_p1) on the 10−100 μs time scale.

The present calculations predict that R5 is the second-largest channel in the JP-10 pyrolysis yielding, at the temperatures and pressures of interest, 28.7−31.4% of the decomposition products. While R5 mainly decomposes to the cyclic C5 fragments, it is also a source of the experimentally observed vinyl and allyl radicals. Ethylene and cyclopentadiene are the major closed-shell molecules predicted here in the R5 decomposition. The fact that the cyclopentenyl isomers predicted by the present calculations were not observed in ALS implicates their fast transformation to C5 cyclic closed-shell molecules cyclopentadiene (via H loss) or cyclopentene (via H addition). R5 also contributes to the formation of the trace acetylene and cyclohexadiene products. Fulveneallene can be produced through dehydrogenation of 3-vinyl-1-cyclopentene R5−1_p1. Because of the higher barriers, the primary decomposition of R5 was calculated to be 1 order of magnitude slower than that of R1 and R4 at 1000 K. However, when the temperature is higher than 1500 K, the differences in the rate constants for these decompositions become small.

3.5. The R6 Radical. The primary decomposition of R6 starts with the C−C bond β-scission breaking the tricyclic framework to produce the R6−1 radical intermediate over a 141 kJ mol^{-1} barrier (Figure 1).[40] Next, there are two competing channels of the primary dissociation (Scheme 4). R6−1 can undergo a direct fragmentation to allyl, C_3H_5 + C_7H_{10} (R6−1_p1). The alternative product, ethylene, C_2H_4 +

DOI: 10.1021/acs.jpca.8b02934
J. Phys. Chem. A 2018, 122, 4920−4934

Scheme 4. Primary and Secondary Channels of Decomposition of R6-1

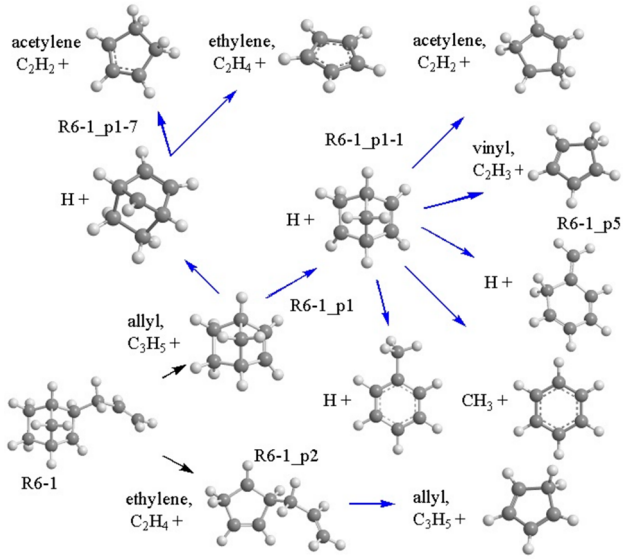

C_8H_{11} (R6−1_p2) is produced first by C−C β-scission, which breaks another five-member ring followed by second C−C β-scission eliminating C_2H_4. The calculated rate constant for the primary decomposition of the R6 radical (Figure 4) increases from 1.4×10^5 s^{-1} at 1000 K to 9.0×10^9 s^{-1} at 2500 K. This is the slowest decomposition among all $C_{10}H_{15}$ fragments of JP-10 considered in this work. Temperatures above 1000 K are needed for the full decomposition of R6 to the primary products on the 10−100 μs time scale. The temperature dependence of the calculated branching ratios of the R6−1_p1 and R6−1_p2 products (Table 11) shows that elevated temperatures result in a more even mixture of these products, whereas at temperatures closer to 1000 K, allyl, C_3H_5 + C_7H_{10} (R6−1_p1) is the main product.

Both radical C_8H_{11} (R6−1_p2) and closed-shell C_7H_{10} (R6−1_p1) fragments were not observed in the ALS experiment, as they have likely underwent secondary decomposition. The C_8H_{11} (R6−1_p2) radical fragment dissociates further to allyl, C_3H_5 + cyclopentadiene, C_5H_6.[40] The calculated rate constant for this reaction is shown in Figure 8. In this work we updated our previous study[40] of the PES for the secondary decomposition of the closed-shell fragment C_7H_{10} (R6−1_p1). The result is shown in Figure S6 (Supporting Information). Among four possible decomposition pathways of C_7H_{10} (R6−1_p1) initiated by a cleavage of a C−H bond we considered only two channels corresponding to the weakest C−H bonds. These pathways lead to the bicyclic C_7H_9 radical fragments R6−1_p1−1 and R6−1_p1−7 (Scheme 4) with the computed strengths of the cleaved C−H bond being 401 and 431 kJ mol^{-1}, respectively. After the C−H bond cleavage, R6−1_p1−1 can undergo further decomposition via two competitive C−C bond β-scissions. One results in reformation of

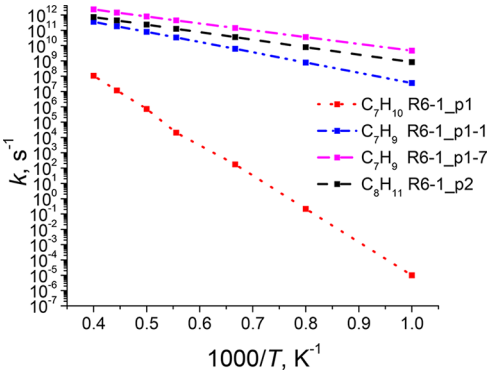

Figure 8. Calculated rate constants for the secondary decompositions in the R6 channel.

the bicyclic structure into a six-member ring structure, which consequently decomposes to the H + 5-methylene-1,3-cyclohexadiene, C_7H_8 (R6−1_p5), H + toluene, C_7H_8 (R6−1_p10) and methyl, CH_3 + benzene, C_6H_6 products. Alternatively, the other C−C bond β-scission can transform R6−1_p1−1 into a five-member ring structure, which would yield the acetylene, C_2H_2 + 3-cyclopentenyl, C_5H_7 and vinyl, C_2H_3+ cyclopentadiene, C_5H_6 products. R6−1_p1−7 also has two competitive C−C bond β-scission channels both leading to five-member ring structures and then to the acetylene, C_2H_2 + 2-cyclopentenyl, C_5H_7 and ethylene, C_2H_4 + cyclopentadienyl, C_5H_5 products. The calculated temperature dependences for the rate constants for the secondary decompositions of the C_7H_{10} (R6−1_p1), C_7H_9 (R6−1_p1−1), and C_7H_9 (R6−1_p1−7) fragments are shown in Figure 8. The results predict that the full decomposition of the closed-shell fragment C_7H_{10} (R6−1_p1) is not expected on the 10−100 μs time scale, if the temperature is below 1600 K. The temperature dependence of the calculated branching ratios for the products of the secondary decomposition of C_7H_{10} (R6−1_p1) is shown in Table 12. The total yield of the products containing the C_6H_x fragments drops from 57% at 1000 K to 39% at 2500 K. At higher temperatures the C_6H_x-containing products are replaced by the products containing the C_5H_x fragments.

In summary, the computational results predict that the decomposition of R6 is the main channel of the JP-10 pyrolysis. At the temperatures and pressures of interest R6 contributes ~50% to the molecular inventory of the pyrolytic process. R6 is predicted to be a significant source of the abundant in the ALS experiment allyl radical, ethylene, and cyclopentadiene. R6 is also a source of methyl, vinyl, cyclopentadienyl, cyclopentenyl radicals as well as acetylene, benzene, toluene, and 5-methylene-1,3-cyclohexadiene closed-shell molecules. The calculated rate constant for the primary decomposition of R6 is somewhat lower than those for R1, R4, and R5 channels. Also, the secondary decomposition of C_7H_{10} in the significant channel R6−1_p1 is predicted by the present calculations to be the rate-limiting process.

Table 11. Calculated Branching Ratio for the Primary Decomposition of R6

	temprature						
product	1000 K	1250 K	1500 K	1750 K	2000 K	2250 K	2500 K
C_3H_5+C_7H_{10} (R6−1_p1)	87.9	70.4	60.3	56.1	54.4	53.7	53.3
C_2H_4+C_8H_{11} (R6−1_p2)	12.1	29.6	39.7	43.9	45.6	46.3	46.7

DOI: 10.1021/acs.jpca.8b02934
J. Phys. Chem. A 2018, 122, 4920−4934

Table 12. Calculated Branching Ratios for the Secondary Decomposition of C_7H_{10} (R6-1_p1)

product	temperature						
	1000 K	1250 K	1500 K	1750 K	2000 K	2250 K	2500 K
H + H + toluene, C_7H_8	1.3	1.4	1.4	1.4	1.3	1.4	1.3
H + H + C_7H_8 (R6−1_p5)	31.5	34.3	33.3	32.0	31.2	30.5	29.7
H + CH_3 + benzene, C_6H_6	24.1	18.3	14.0	11.1	9.8	8.6	7.7
H + C_2H_2 + cyclopentenyl, C_5H_7	1.1	7.0	15.0	20.2	22.0	23.4	24.5
H + C_2H_3 + cyclopentadiene, C_5H_6	39.6	34.0	29.1	25.8	24.4	23.2	22.2
H + C_2H_4 + cyclopentadienyl, C_5H_5	2.6	4.9	7.3	9.5	11.4	13.0	14.4

4. DISCUSSION AND CONCLUSIONS

Our previously published calculations of PESs for the JP-10 pyrolysis[40] allowed us to outline the possible reaction mechanisms leading to all products observed in the short-residence-time ALS experiment. The calculations of the rate constants and product branching ratios presented here make possible a more quantitative assessment of the previously outlined decomposition mechanisms by a comparison with the experimental data. Table 13 shows the calculated (1500 K, HP limit) and the experimentally measured (ALS, 1500 K) branching ratios for the main part (~95%) of the JP-10 pyrolytic products (the full account including numerous trace products is given in Table S1 in Supporting Information). At 1500 K, the major products predicted by the theoretical modeling are ethylene, C_2H_4, allyl radical, C_3H_5, cyclopentadiene, C_5H_6, and cyclopentenyl radical, C_5H_7. Overall, these results are in general accord with the ALS experimental data. The major radical identified both in the experimental and theoretical studies, allyl C_3H_5, is well-known[76−78] to decompose to allene, C_3H_4, methylacetylene, C_3H_4, and then to the propargyl radical, C_3H_3, and can also recombine with hydrogen atoms to form propene, C_3H_6. Indeed, the computed yield of allyl radical is larger than that measured in ALS, whereas allene is observed experimentally, but no significant yield of this product was found in our calculations. Another difference between the computed and measured branching ratios is that cyclopentenyl radical, C_5H_7, was not detected in experiment, while fulvene, C_6H_6, was not among the major products predicted by the calculations. This difference indicates that cyclopentenyl is not stable under the experimental conditions and likely to undergo further dissociation to cyclopentadiene, C_5H_6, and/or that there are pathways to fulvene competing with those to cyclic C_5H_x products. The pathways to fulvene predicted within the employed theoretical model are secondary decompositions of the C_8H_{11} (R4−1_p1 and R4−3_p2) and C_8H_{10} (R4−3_p1) fragments. However, the calculated total yield of the R4 channel, below 4% at the temperatures and pressures of interest (Table 1), is a limiting factor on the yield of fulvene by these channels. The difference between the experiment and our calculations may be caused by a recombination of the decomposition products, which was not considered within the employed theoretical model. For example, H addition to the vinyl chain of 3-vinyl-1-cyclopentene, C_7H_{10} (R5−1_p1) will create a viable competition for the H loss in this closed-shell molecule, and a significant reaction flux to the cyclic C_5 products can be replaced than by a reaction flux to fulvene.

Table 13. Experimentals Versus the Calculated (1500 K) Branching Ratio for the Main Products of the JP-10 Pyrolysis

species	formula	theory	experiment[40]
methyl	CH_3	2.02	2.73 (−0.61, +0.64)
acetylene	C_2H_2	2.40	0.54 (−0.12, +0.13)
vinyl	C_2H_3	1.43	0.38 (−0.20, +0.42)
ethylene	C_2H_4	12.12	24.59 (−5.21, +5.35)
ethyl	C_2H_5	0.12	2.37 (−0.53, +0.55)
allene	C_3H_4	0.00	2.50 (−0.60, +0.66)
allyl	C_3H_5	24.50	12.95 (−3.11, +3.37)
1,3-butadiene	C_4H_6	1.70	2.49 (−0.53, +0.55)
cyclopentadienyl	C_5H_5	1.07	3.09 (−1.59, +3.27)
cyclopentadiene	C_5H_6	20.57	19.91 (−4.39, +4.60)
cyclopentenyl	C_5H_7	16.05	
cyclopentene	C_5H_8	5.69	2.93 (−0.66, +0.70)
fulvene	C_6H_6	0.64	13.28 (−6.89, +14.28)
benzene	C_6H_6	2.22	4.46 (−0.97, +1.01)
5-methylene-1,3-cyclohexadiene	C_7H_8	4.06	0.73 (−0.38, +0.80)
toluene	C_7H_8	0.17	0.40 (−0.22, +0.46)

While considering the comparison of the calculated and experimental product yields above, we note that there are several factors rendering its validity limited. First, the high-temperature reactor used in the experiment[40] does not feature homogeneous temperature and pressure conditions along its tube. Second, the residence time of the gas flowing through the reactor inside the tube is in the range of hundreds of microseconds, which may be sufficient for a number of primary, secondary, and consequent reactions to occur. Therefore, a direct comparison of the theoretical and experimental product branching ratios can only be possible through the modeling of the gas dynamics inside the reactor's tube generating the temperature, pressure, and gas velocity profiles, coupled with the kinetic modeling of all chemical reactions, which may occur while the gas flows through the reactor. We reported such combined gas dynamics/chemical kinetics modeling in a recent publication on a simpler C_6H_5 + C_4H_4 system.[79] Similar calculations can be, in principle, performed for the JP-10 pyrolysis using the rate constants produced in the present work, but this would be a subject of a separate detailed modeling study planned for the future. Here, we only briefly analyze some general trends in the behavior of the relative yields of the main product groups with temperature and pressure if these conditions were homogeneous in a hypothetical pyrolysis process.

The pressure effect on the rate constant for the decomposition of JP-10 via initial C−H bond cleavages is predicted to become significant at temperatures above 1500 K (Figure 3). Figure 9 shows the calculated temperature dependences of the yields for the main decomposition products when combined into C*n* groups. The C1 group, which consists only of one product, methyl radical, sees a drop from 4.7% to 1.5% when temperature rises from 1000 to 2500 K. The increasing temperature raises the yield of the C2 group from

DOI: 10.1021/acs.jpca.8b02934
J. Phys. Chem. A 2018, 122, 4920−4934

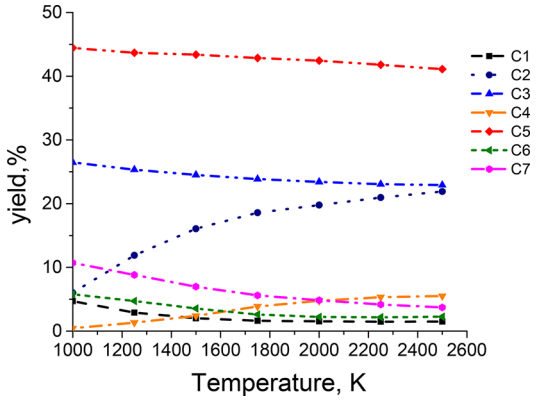

Figure 9. Calculated temperature dependences of the yields for the main decomposition products combined into C*n* groups.

6% at 1000 K to 22% at 2500 K. This increase is caused mainly by increasing yields of acetylene, vinyl radical, and ethylene. Higher temperatures also favor the yield of the C4 group (mainly 1,3-butadiene), which grows from 0.5% at 1000 K to 5.5% at 2500 K. The C5 group sees a relatively small decrease of the yield, from 44.4% at 1000 K to 41.1% at 2500 K. Thus, for all temperatures of interest, C5 is predicted to be the main group in the molecular inventory of the decomposition products of JP-10. The calculated decrease in the combined yield of the C5 products is caused mainly by cyclopentene, while the yields of cyclopentadiene and of cyclopentenyl show little dependence on temperature. It is worth noting that the yield of cyclopentadienyl radical, a minor C5 product, grows with temperature from 0.7% at 1000 K to 1.7% at 2500 K. The combined yield of C6 and C7 groups (mainly fulvene, benzene, toluene, and 5-methylene-1,3-cyclohexadiene) drops from 16.5% at 1000 K to 6% at 2500 K.

In conclusion, the present theoretical calculations show an overall agreement with the results of the short-residence-time ALS experiment, and thus the proposed theoretical approach can be used for more reliable kinetic modeling of JP-10 pyrolysis. The presented calculations of the rate constants and product branching ratios allow identifying the most favorable reaction pathways to the most important fragmentation products depending on the temperature regime of the pyrolytic process. In accord with the ALS experiment, the calculations predict that on the 10−100 μs time scale the important decomposition fragments are methyl radical, acetylene, vinyl radical, ethyl radical, ethylene, allyl radical, 1,3-butadiene, cyclopentadienyl radical, cyclopentadiene, cyclopentenyl radical, cyclopentene, fulvene, benzene, toluene, and 5-methylene-1,3-cyclohexadiene. The calculations showed that ethylene, allyl radical, cyclopentadiene, and cyclopentenyl radical are significant products at all temperatures of interest, while the inventory of other products depends to a large extent on the temperature of the pyrolysis. With the increasing temperature the strongest trends are an increase of the yields in the C2 and C4 groups and a decrease of the yields in the C1, C6, and C7 groups. One can expect that the initially produced radicals will react away to form closed-shell molecules. Indeed, the predominant fragments observed in our long-residence-time experiment, 120−140 ms, were ethylene, propene, cyclopentadiene, cyclopentene, fulvene, and benzene.[40] Therefore, the oxidation mechanism of JP-10 is expected to depend significantly both on the temperature of the pyrolysis and on the time when the oxidation process begins.

We expect that the rate constants and product branching ratios for the key reactions calculated here should improve the existing kinetic models for the JP-10 pyrolysis like the one developed by Vandewiele et al.[17] and eventually render them with predictive power. In the meantime, since the agreement of the calculated product branching ratios with the experimental values still is not quantitative (at least for some of the products), further improvements can be made in the future. For instance, the unimolecular reactions considered in the present mechanism can be augmented with bimolecular reactions, which can be fast enough to occur on the 10−100 μs time scale. Here, H abstraction reactions with H atoms and especially H-facilitated (H-assisted) isomerization and dissociation channels might play an important role due to a high expected concentration of H atoms if the pyrolysis is initiated by C−H bond cleavages in the parent molecule. The inclusion of the H-assisted reactions perhaps should be the next significant step in the development of an accurate kinetic model for the JP-10 pyrolysis and consequent oxidation.

■ ASSOCIATED CONTENT

Supporting Information

The Supporting Information is available free of charge on the ACS Publications website at DOI: 10.1021/acs.jpca.8b02934.

Figures depicting potential energy diagrams for secondary decomposition channels calculated in the present study; tabulated experimental values versus the calculated (1500 K) branching ratios for the products of the JP-10 pyrolysis; optimized Cartesian coordinates and calculated vibrational frequencies of all stationary structures used in rate constant calculations (PDF)

■ AUTHOR INFORMATION

Corresponding Authors

*E-mail: Ralfk@hawaii.edu. (R.I.K.)
*E-mail: Mebela@fiu.edu. (A.M.M.)

ORCID

Alexander M. Mebel: 0000-0002-7233-3133
Ralf I. Kaiser: 0000-0002-7233-7206

Notes

The authors declare no competing financial interest.

■ ACKNOWLEDGMENTS

This project is supported by the Air Force Office of Scientific Research under Grant No. FA9550-15-1-0011.

■ REFERENCES

(1) Osmont, A.; Gokalp, I.; Catoire, L. Evaluating Missile Fuels. *Propellants, Explos., Pyrotech.* **2006**, *31*, 343−354.
(2) Chung, H.; Chen, C.; Kremer, R.; Boulton, J.; Burdette, G. Recent Developments in High-Energy Density Liquid Hydrocarbon Fuels. *Energy Fuels* **1999**, *13*, 641−649.
(3) Maurice, L. Q.; Lander, H.; Edwards, T.; Harrison, W. Advanced Aviation Fuels: A Look Ahead via a Historical Perspective. *Fuel* **2001**, *80*, 747−756.
(4) Van Devener, B.; Anderson, S. L. Breakdown and Combustion of JP-10 Fuel Catalyzed by Nanoparticulate CeO_2 and Fe_2O_3. *Energy Fuels* **2006**, *20*, 1886−1894.
(5) Gao, C. W.; Vandeputte, A. G.; Yee, N. W.; Green, W. H.; Bonomi, R. E.; Magoon, G. R.; Wong, H.-W.; Oluwole, O. O.; Lewis, D. K.; Vandewiele, N. M.; et al. JP-10 Combustion Studied with Shock Tube Experiments and Modeled with Automatic Reaction Mechanism Generation. *Combust. Flame* **2015**, *162*, 3115−3129.

(6) Nakra, S.; Green, R. J.; Anderson, S. L. Thermal Decomposition of JP-10 Studied By Micro-Flowtube Pyrolysis-Mass Spectrometry. *Combust. Flame* **2006**, *144*, 662−674.
(7) Vandewiele, N. M.; Magoon, G. R.; Van Geem, K. M.; Reyniers, M.-F.; Green, W. H.; Marin, G. B. Experimental and Modeling Study on the Thermal Decomposition of Jet Propellant-10. *Energy Fuels* **2014**, *28*, 4976−4985.
(8) Herbinet, O.; Sirjean, B.; Bounaceur, R.; Fournet, R.; Battin-Leclerc, F.; Scacchi, G.; Marquaire, P.-M. Primary Mechanism of the Thermal Decomposition of Tricyclodecane. *J. Phys. Chem. A* **2006**, *110*, 11298−11314.
(9) Nageswara Rao, P.; Kunzru, D. Thermal Cracking of JP-10: Kinetics And Product Distribution. *J. Anal. Appl. Pyrolysis* **2006**, *76*, 154−160.
(10) Striebich, R.; Lawrence, J. Thermal Decomposition of High-Energy Density Materials at High Pressure and Temperature. *J. Anal. Appl. Pyrolysis* **2003**, *70*, 339−352.
(11) Wohlwend, K.; Maurice, L.; Edwards, T.; Striebich, R.; Vangsness, M.; Hill, A. Thermal Stability of Energetic Hydrocarbon Fuels for Use in Combined Cycle Engines. *J. Propul. Power* **2001**, *17*, 1258−1262.
(12) Xing, Y.; Fang, W.; Xie, W.; Guo, Y.; Lin, R. Thermal Cracking of JP-10 under Pressure. *Ind. Eng. Chem. Res.* **2008**, *47*, 10034−10040.
(13) Li, G.; Zhang, C.; Wei, H.; Xie, H.; Guo, Y.; Fang, W. Investigations on the Thermal Decomposition of JP-10/*iso*-Octane Binary Mixtures. *Fuel* **2016**, *163*, 148−156.
(14) Bruno, T. J.; Huber, M. L.; Laesecke, A.; Lemmon, E. W.; Perkins, R. A. Thermochemical and Thermophysical Properties of JP-10. *Technol. Rep. NISTIR* **2006**, *6640*, 325.
(15) Park, S. H.; Kwon, C. H.; Kim, J.; Chun, B. H.; Kang, J. W.; Han, J. S.; Jeong, B. H.; Kim, S. H. Thermal Stability and Isomerization Mechanism of exo-Tetrahydrodicyclopentadiene: Experimental Study and Molecular Modeling. *Ind. Eng. Chem. Res.* **2010**, *49*, 8319−8324.
(16) Li, H.; Liu, G.; Jiang, R.; Wang, L.; Zhang, X. Experimental and Kinetic Modeling Study of exo-TCD Pyrolysis under Low Pressure. *Combust. Flame* **2015**, *162*, 2177−2190.
(17) Vandewiele, N. M.; Magoon, G. R.; Van Geem, K. M.; Reyniers, M.-F.; Green, W. H.; Marin, G. B. Kinetic Modeling of Jet Propellant-10 Pyrolysis. *Energy Fuels* **2015**, *29*, 413−427.
(18) Yue, L.; Xie, H.-J.; Qin, X.-M.; Lu, X.-X.; Fang, W.-J. A DFT Study on the Thermal Cracking of JP-10. *J. Mol. Model.* **2013**, *19*, 5355−5365.
(19) Chenoweth, K.; van Duin, A. C. T.; Dasgupta, S.; Goddard Iii, W. A. Initiation Mechanisms and Kinetics of Pyrolysis and Combustion of JP-10 Hydrocarbon Jet Fuel. *J. Phys. Chem. A* **2009**, *113*, 1740−1746.
(20) Magoon, G. R.; Aguilera-Iparraguirre, J.; Green, W. H.; Lutz, J. J.; Piecuch, P.; Wong, H. W.; Oluwole, O. O. Detailed Chemical Kinetic Modeling of JP-10 (*exo*-Tetrahydrodicyclopentadiene) High-Temperature Oxidation: Exploring the Role of Biradical Species in Initial Decomposition Steps. *Int. J. Chem. Kinet.* **2012**, *44*, 179−193.
(21) Hudzik, J. M.; Asatryan, R.; Bozzelli, J. W. Thermochemical Properties of exo-Tricyclo 5.2.1.0(2,6) decane (JP-10 Jet Fuel) and Derived Tricyclodecyl Radicals. *J. Phys. Chem. A* **2010**, *114*, 9545−9553.
(22) Hudzik, J. M.; Castillo, A.; Bozzelli, J. W. Bond Energies and Thermochemical Properties of Ring-Opened Diradicals and Carbenes of exo-Tricyclo 5.2.1.0(2,6) decane. *J. Phys. Chem. A* **2015**, *119*, 9857−9878.
(23) Zehe, M. J.; Jaffe, R. L. Theoretical Calculation of Jet Fuel Thermochemistry. 1. Tetrahydrodicylopentadiene (JP10) Thermochemistry Using the CBS-QB3 and G3(MP2)//B3LYP Methods. *J. Org. Chem.* **2010**, *75*, 4387−4391.
(24) Cheng, S. S.; Liou, K. F.; Lin, Y. T. High-Energy Fuels 0.1. A Novel Preparation of Exo-Tetrahydrodicyclopentadiene by Isomerization of Endo-Tetrahydrodicyclopentadiene. *J. Chin. Chem. Soc.* **1986**, *33*, 335−340.
(25) Prakash, O.; Tiwari, R. K.; Kalra, S. L.; Venkataramani, P. S. Isomerization of Endo-Tetrahydrodicyclopentadiene to Exo-Tetrahydrodicyclopentadiene. *Indian J. Chem. Technol.* **1995**, *2*, 295−297.
(26) Davidson, D. F.; Horning, D. C.; Herbon, J. T.; Hanson, R. K. Shock Tube Measurements of JP-10 Ignition. *Proc. Combust. Inst.* **2000**, *28*, 1687−1692.
(27) Li, S. C.; Varatharajan, B.; Williams, F. A. Chemistry of JP-10 Ignition. *AIAA J.* **2001**, *39*, 2351−2356.
(28) Mikolaitis, D. W.; Segal, C.; Chandy, A. Ignition Delay for Jet Propellant 10/Air and Jet Propellant 10/High-Energy Density Fuel/Air Mixtures. *J. Propul. Power* **2003**, *19*, 601−606.
(29) Parsinejad, F.; Arcari, C.; Metghalchi, H. Flame Structure and Burning Speed of JP-10 Air Mixtures. *Combust. Sci. Technol.* **2006**, *178*, 975−1000.
(30) Jiao, C. Q.; DeJoseph, C. A.; Garscadden, A. Dissociative Ionization of JP-10 ($C_{10}H_{16}$) by Electron Impact. *Int. J. Mass Spectrom.* **2007**, *266*, 92−96.
(31) Wang, S.; Gou, H.-j.; Fan, B.-c.; He, Y.-z.; Zhang, S.-t.; Cui, J.-p. Shock Tube Study of JP-10 Ignition Delay Time. *Chin. J. Chem. Phys.* **2007**, *20*, 48−52.
(32) Xing, Y.; Guo, Y. S.; Li, D.; Fang, W. J.; Lin, R. S. Measurement of Bubble-Point Vapor Pressure for Systems of JP-10 with Ethanol. *Energy Fuels* **2007**, *21*, 1048−1051.
(33) Yang, F. J.; Guo, Y. S.; Xing, Y.; Li, D.; Fang, W. J.; Lin, R. S. Densities and Viscosities of Binary Mixtures of JP-10 with *n*-Octane or *n*-Decane at Several Temperatures. *J. Chem. Eng. Data* **2008**, *53*, 2237−2240.
(34) Su, X. H.; Hou, H. M.; Li, G.; Lin, R. S.; Cai, S. L. Product Distribution of Thermal Cracking of exo-Tetrahydrodicyclopentadiene. *Acta. Chimica. Sinica.* **2009**, *67*, 587−592.
(35) Seiser, R.; Niemann, U.; Seshadri, K. Experimental Study of Combustion of *n*-Decane and JP-10 in non-Premixed Flows. *Proc. Combust. Inst.* **2011**, *33*, 1045−1052.
(36) Guo, F.; Cheng, X. L.; Zhang, H. Reaxff Molecular Dynamics Study of Initial Mechanism of JP-10 Combustion. *Combust. Sci. Technol.* **2012**, *184*, 1233−1243.
(37) Goh, K. H. H.; Geipel, P.; Hampp, F.; Lindstedt, R. P. Regime Transition from Premixed to Flameless Oxidation in Turbulent JP-10 Flames. *Proc. Combust. Inst.* **2013**, *34*, 3311−3318.
(38) Türker, L.; Variş, S.; Çelik Bayar, Ç. A Theoretical Study of JP-10 Hydroperoxidation. *Fuel* **2013**, *104*, 128−132.
(39) Qin, X. M.; Xie, H. J.; Yue, L.; Lu, X. X.; Fang, W. J. A Quantum Chemistry Study on Thermochemical Properties of High Energy-Density Endothermic Hydrocarbon Fuel JP-10. *J. Mol. Model.* **2014**, *20*, 2183.
(40) Zhao, L.; Yang, T.; Kaiser, R. I.; Troy, T. P.; Xu, B.; Ahmed, M.; Alarcon, J.; Belisario-Lara, D.; Mebel, A. M.; Zhang, Y.; et al. A Vacuum Ultraviolet Photoionization Study on High-Temperature Decomposition of JP-10 (*exo*-Tetrahydrodicyclopentadiene). *Phys. Chem. Chem. Phys.* **2017**, *19*, 15780−15807.
(41) Zhang, F. T.; Kaiser, R. I.; Kislov, V. V.; Mebel, A. M.; Golan, A.; Ahmed, M. A VUV Photoionization Study of the Formation of the Indene Molecule and Its Isomers. *J. Phys. Chem. Lett.* **2011**, *2*, 1731−1735.
(42) Zhang, F. T.; Kaiser, R. I.; Golan, A.; Ahmed, M.; Hansen, N. A VUV Photoionization Study of the Combustion-Relevant Reaction of the Phenyl Radical (C_6H_5) with Propylene (C_3H_6) in a High Temperature Chemical Reactor. *J. Phys. Chem. A* **2012**, *116*, 3541−3546.
(43) Kaiser, R. I.; Belau, L.; Leone, S. R.; Ahmed, M.; Wang, Y. M.; Braams, B. J.; Bowman, J. M. A Combined Experimental and Computational Study on the Ionization Energies of the Cyclic and Linear C_3H Isomers. *ChemPhysChem* **2007**, *8*, 1236−1239.
(44) Kaiser, R. I.; Mebel, A.; Kostko, O.; Ahmed, M. On the Ionization Energies of C_4H_3 Isomers. *Chem. Phys. Lett.* **2010**, *485*, 281−285.
(45) Kaiser, R. I.; Maksyutenko, P.; Ennis, C.; Zhang, F. T.; Gu, X. B.; Krishtal, S. P.; Mebel, A. M.; Kostko, O.; Ahmed, M. Untangling the Chemical Evolution of Titan's Atmosphere and Surface-from

DOI: 10.1021/acs.jpca.8b02934
J. Phys. Chem. A 2018, 122, 4920−4934

Homogeneous to Heterogeneous Chemistry. *Faraday Discuss.* **2010**, *147*, 429−478.
(46) Kaiser, R. I.; Sun, B. J.; Lin, H. M.; Chang, A. H. H.; Mebel, A. M.; Kostko, O.; Ahmed, M. An Experimental and Theoretical Study of the Ionization Energies of Polyynes (H-(C≡C)$_n$-H;n= 1−9). *Astrophys. J.* **2010**, *719*, 1884−1889.
(47) Kostko, O.; Zhou, J.; Sun, B. J.; Lie, J. S.; Chang, A. H. H.; Kaiser, R. I.; Ahmed, M. Determination of Ionization Energies of C_nN (n= 4−12): Vacuum Ultraviolet Photoionization Experiments and Theoretical Calculations. *Astrophys. J.* **2010**, *717*, 674−682.
(48) Kaiser, R. I.; Krishtal, S. P.; Mebel, A. M.; Kostko, O.; Ahmed, M. An Experimental and Theoretical Study of the Ionization Energies of SiC_2H_x(x= 0, 1, 2) Isomers. *Astrophys. J.* **2012**, *761*, 178−184.
(49) Golan, A.; Ahmed, M.; Mebel, A. M.; Kaiser, R. I. A VUV Photoionization Study of the Multichannel Reaction of Phenyl Radicals with 1,3-Butadiene under Combustion Relevant Conditions. *Phys. Chem. Chem. Phys.* **2013**, *15*, 341−347.
(50) Parker, D. S.; Kaiser, R. I.; Troy, T. P.; Ahmed, M. Hydrogen Abstraction/Acetylene Addition Revealed. *Angew. Chem., Int. Ed.* **2014**, *53*, 7740−7744.
(51) Qi, F.; Yang, R.; Yang, B.; Huang, C. Q.; Wei, L. X.; Wang, J.; Sheng, L. S.; Zhang, Y. W. Isomeric Identification of Polycyclic Aromatic Hydrocarbons Formed in Combustion with Tunable Vacuum Ultraviolet Photoionization. *Rev. Sci. Instrum.* **2006**, *77*, 084101.
(52) Yang, B.; Li, Y. Y.; Wei, L. X.; Huang, C. Q.; Wang, J.; Tian, Z. Y.; Yang, R.; Sheng, L. S.; Zhang, Y. W.; Qi, F. An Experimental Study of The Premixed Benzene/Oxygen/Argon Flame with Tunable Synchrotron Photoionization. *Proc. Combust. Inst.* **2007**, *31*, 555−563.
(53) Yang, B.; Oswald, P.; Li, Y.; Wang, J.; Wei, L.; Tian, Z.; Qi, F.; Kohse-Höinghaus, K. Identification of Combustion Intermediates in Isomeric Fuel-Rich Premixed Butanol−Oxygen Flames at Low Pressure. *Combust. Flame* **2007**, *148*, 198−209.
(54) Li, Y. Y.; Zhang, L. D.; Tian, Z. Y.; Yuan, T.; Wang, J.; Yang, B.; Qi, F. Experimental Study of a Fuel-Rich Premixed Toluene Flame at Low Pressure. *Energy Fuels* **2009**, *23*, 1473−1485.
(55) Li, Y. Y.; Zhang, L. D.; Tian, Z. Y.; Yuan, T.; Zhang, K. W.; Yang, B.; Qi, F. Investigation of the Rich Premixed Laminar Acetylene/Oxygen/Argon Flame: Comprehensive Flame Structure and Special Concerns of Polyynes. *Proc. Combust. Inst.* **2009**, *32*, 1293−1300.
(56) Zhang, L. D.; Cai, J. H.; Zhang, T. C.; Qi, F. Kinetic Modeling Study of Toluene Pyrolysis at Low Pressure. *Combust. Flame* **2010**, *157*, 1686−1697.
(57) Oßwald, P.; Güldenberg, H.; Kohse-Höinghaus, K.; Yang, B.; Yuan, T.; Qi, F. Combustion of Butanol Isomers − A Detailed Molecular Beam Mass Spectrometry Investigation of Their Flame Chemistry. *Combust. Flame* **2011**, *158*, 2−15.
(58) Qi, F. Combustion Chemistry Probed by Synchrotron VUV Photoionization Mass Spectrometry. *Proc. Combust. Inst.* **2013**, *34*, 33−63.
(59) Curtiss, L. A.; Raghavachari, K.; Redfern, P. C.; Rassolov, V.; Pople, J. A. Gaussian-3 (G3) Theory for Molecules Containing First and Second-Row Atoms. *J. Chem. Phys.* **1998**, *109*, 7764−7776.
(60) Curtiss, L. A.; Raghavachari, K.; Redfern, P. C.; Baboul, A. G.; Pople, J. A. Gaussian-3 Theory Using Coupled Cluster Energies. *Chem. Phys. Lett.* **1999**, *314*, 101−107.
(61) Baboul, A. G.; Curtiss, L. A.; Redfern, P. C.; Raghavachari, K. Gaussian-3 Theory Using Density Functional Geometries and Zero-Point Energies. *J. Chem. Phys.* **1999**, *110*, 7650−7657.
(62) Frisch, M. J.; Trucks, G. W.; Schlegel, H. B.; Scuseria, G. E.; Robb, M. A.; Cheeseman, J. R.; Scalmani, G.; Barone, V.; Mennucci, B.; Petersson, G. A.; et al. *Gaussian 09, Revision A.1;* Gaussian Inc.: Wallingford, CT, 2009.
(63) Werner, H. J.; Knowles, P. J.; Knizia, G.; Manby, F. R.; Schütz, M.; Celani, P.; Györffy, W.; Kats, D.; Korona, T.; Lindh, R.; et al. MOLPRO, version 2010.1, a package of ab initio programs, http://www.molpro.net.
(64) Marcus, R. A. Unimolecular Dissociations and Free Radical Recombination Reactions. *J. Chem. Phys.* **1952**, *20*, 359−364.
(65) Georgievskii, Y.; Klippenstein, S. J. Transition State Theory for Multichannel Addition Reactions: Multifaceted Dividing Surfaces. *J. Phys. Chem. A* **2003**, *107*, 9776−9781.
(66) Celani, P.; Werner, H.-J. Multireference Perturbation Theory for Large Restricted and Selected Active Space Reference Wave Functions. *J. Chem. Phys.* **2000**, *112*, 5546−5557.
(67) Shiozaki, T.; Gyorffy, W.; Celani, P.; Werner, H.-J. Extended Multi-State Complete Active Space Second-Order Perturbation Theory: Energy and Nuclear Gradients. *J. Chem. Phys.* **2011**, *135*, 081106.
(68) Dunning, T. H., Jr. Gaussian Basis Sets for Use in Correlated Molecular Calculations. I. The Atoms Boron through Neon and Hydrogen. *J. Chem. Phys.* **1989**, *90*, 1007−1023.
(69) Georgievskii, Y.; Miller, J. A.; Klippenstein, S. J. Association Rate Constants for Reactions Between Resonance-Stabilized Radicals: C_3H_3 + C_3H_3, C_3H_3 + C_3H_5, and C_3H_5 + C_3H_5. *Phys. Chem. Chem. Phys.* **2007**, *9*, 4259−4268.
(70) Georgievskii, Y.; Miller, J. A.; Burke, M. P.; Klippenstein, S. J. Reformulation and Solution of the Master Equation for Multiple-Well Chemical Reactions. *J. Phys. Chem. A* **2013**, *117*, 12146−12154.
(71) Georgievskii, Y.; Klippenstein, S. J. MESS Program Package, 2015, http://tcg.cse.anl.gov/papr.
(72) Zhao, L.; Yang, T.; Kaiser, R. I.; Troy, T. P.; Ahmed, M.; Belisario-Lara, D.; Ribeiro, J. M.; Mebel, A. M. Combined Experimental and Computational Study on the Unimolecular Decomposition of JP-8 Jet Fuel Surrogates. I. n-Decane (n-$C_{10}H_{22}$). *J. Phys. Chem. A* **2017**, *121*, 1261−1280.
(73) Jasper, A. W.; Oana, C. M.; Miller, J. A. Third-Body" Collision Efficiencies for Combustion Modeling: Hydrocarbons in Atomic and Diatomic Baths. *Proc. Combust. Inst.* **2015**, *35*, 197−204.
(74) Troe, J. Theory of Thermal Unimolecular Reactions at Low-Pressures. 1. Solutions of master equation. *J. Chem. Phys.* **1977**, *66*, 4745−4757.
(75) Krasnoukhov, V. S.; Porfiriev, D. P.; Zavershinskiy, I. P.; Azyazov, V. N.; Mebel, A. M. Kinetics of the CH_3 + C_5H_5 Reaction: A Theoretical Study. *J. Phys. Chem. A* **2017**, *121*, 9191−9200.
(76) Narendrapurapu, B. S.; Simmonett, A. C.; Schaefer, H. F., III; Miller, J. A.; Klippenstein, S. J. Combustion Chemistry: Important Features of the C_3H_5 Potential Energy Surface, Including Allyl Radical, Propargyl + H_2, Allene + H, and Eight Transition States. *J. Phys. Chem. A* **2011**, *115*, 14209−14214.
(77) Hansen, N.; Miller, J. A.; Westmoreland, P. R.; Kasper, T.; Kohse-Hoinghaus, K.; Wang, J.; Cool, T. A. Isomer-Specific Combustion Chemistry in Allene and Propyne Flames. *Combust. Flame* **2009**, *156*, 2153−2164.
(78) Miller, J. A.; Senosiain, J. P.; Klippenstein, S. J.; Georgievskii, Y. Reactions over Multiple, Interconnected Potential Wells: Unimolecular and Bimolecular Reactions on a C_3H_5 Potential. *J. Phys. Chem. A* **2008**, *112*, 9429−9438.
(79) Zhao, L.; Kaiser, R. I.; Xu, B.; Ablikim, U.; Ahmed, M.; Zagidullin, M. V.; Azyazov, V. N.; Howlader, A. H.; Wnuk, S. F.; Mebel, A. M. VUV Photoionization Study of the Formation of the Simplest Polycyclic Aromatic Hydrocarbon: Naphthalene ($C_{10}H_8$). *J. Phys. Chem. Lett.* **2018**, *9*, 2620−2626.

DOI: 10.1021/acs.jpca.8b02934
J. Phys. Chem. A 2018, 122, 4920−4934